Environmental Science & Technology

Article

pubs.acs.org/est

# Fe(III) Nucleation in the Presence of Bivalent Cations and Oxyanions Leads to Subnanoscale 7 Å Polymers

Case M. van Genuchten,*[,†,⊥] Ashok J. Gadgil,[†,‡] and Jasquelin Peña[§]

[†]Department of Civil and Environmental Engineering, University of California, Berkeley, Berkeley, California 94720, United States
[‡]Environmental Energy Technologies Division, Lawrence Berkeley National Laboratory, Berkeley, California 94720, United States
[§]Institut de Dynamiques de la Surface Terrestre, University of Lausanne, Lausanne 1015, Switzerland

Supporting Information

**ABSTRACT:** Highly disordered Fe(III) phases formed in the presence of bivalent cations and oxyanions represent important components of the global Fe cycle due to their potential for rapid turnover and their critical roles in controlling the speciation of major and trace elements. However, a poor understanding of the formation pathway and structure of these Fe phases has prevented assessments of their thermodynamic properties and biogeochemical reactivity. In this work, we derive structural models for the Fe(III)−As(V)−Ca and Fe(III)−P−Ca polymers formed from Fe(II) oxidation and Fe(III) polymerization in the presence of As(V)/P and Ca. The polymer phase consists of a less than 7 Å coherent network of As(V)/P coordinated to Fe(III) polyhedra, with varying amounts of Ca bound directly and indirectly to the oxyanion. This phase forms at the onset of Fe(II) oxidation and, because of its large oxyanion:Fe solids ratio, depletes the oxyanion concentration with only small amounts of Fe. Our results demonstrate that when a steady supply of Fe(III) is provided from an Fe(II) source, these Fe(III) polymers, which dominate oxyanion uptake, form with little dependence on the initial oxyanion concentration. The formation mechanisms and structures of the oxyanion-rich Fe(III) polymers determined in this study enable future thermodynamic investigations of these phases, which are required to model the interrelated biogeochemical cycles of Fe, As(V)/P, and Ca.

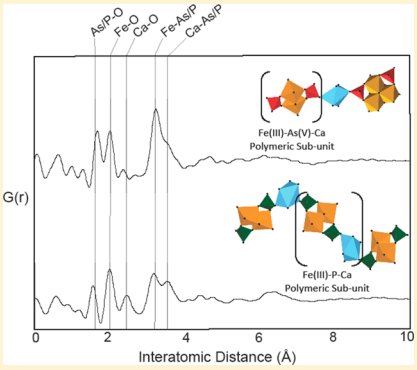


## INTRODUCTION

Disordered Fe(III) phases rich in oxyanions and bivalent cations represent important components of the global Fe cycle. Short-range ordered Fe(III) phases containing arsenate ($H_2AsO_4^-/HAsO_4^{2-}$) or phosphate ($H_2PO_4^-/HPO_4^{2-}$) form in a diverse range of pristine and contaminated aquatic systems such as freshwater lakes;[1] marine and brackish waters;[2] oxic−anoxic boundaries in soils, sediments, and groundwater[3,4] hydrothermal vents;[5] and mining-impacted environments.[6] Relative to nanocrystalline Fe(III) minerals such as 2-line ferrihydrite, these phases show even less structural coherence and a reduced crystallite size,[5,6] which leads to their enhanced capacity for oxyanion uptake.[7] Furthermore, owing to their extreme disorder, the Fe(III) phases formed in the presence of bivalent cations and oxyanions are susceptible to rapid dissolution and phase transformation.[6,8−10] These physical and chemical properties strongly suggest a structure consisting of a polymeric arrangement of Fe(III) polyhedra. However, the positions of atoms and the extent of coherent bonding within the polymers are not known.

The formation and composition of short-range ordered Fe(III) phases are governed by the interaction between Ca and As(V)/P oxyanions during Fe(III) hydrolysis and nucleation. However, the literature offers contradictory accounts of the effect of Ca on Fe−Fe polymerization in oxyanion-rich solutions. For example, Ca enhances the uptake of surface-poisoning As(V) and P oxyanions,[11−13] which are well-known to disrupt Fe−Fe polymerization.[7,14] Yet, spectroscopic studies report that increasing Ca concentrations in P- and As(V)-containing solutions leads to an increase in the average number of Fe−Fe near-neighbors[4] and a transition to more crystalline Fe(III) phases.[12] This apparent contradiction between Ca-enhanced oxyanion uptake and increase in crystallinity can be reconciled by the existence of a separate polymeric phase that dominates oxyanion uptake, but that cannot be detected with standard solid-phase characterization techniques.

The structure of polymeric Fe(III) phases has not been determined due to a combination of confounding factors. First, Fe(III) polymers are frequently admixed with more crystalline Fe(III) minerals in natural and model laboratory systems.[1,3,10,15] In these cases, the weak spectroscopic or diffraction signal produced by the polymer is overlooked or included as disorder in the structural model of the crystalline mineral. Second, even if the polymers can be isolated,[16] the lack of structural order beyond one or two coordination spheres renders their characterization difficult. Although widely used, Fe K-edge extended X-ray absorption fine structure (EXAFS)

Received: July 7, 2014
Revised: September 17, 2014
Accepted: September 19, 2014
Published: September 19, 2014

spectroscopy is limited because of the difficulty in interpreting the contribution of multiple, overlapping atomic paths to the X-ray absorption spectrum of nanocrystalline material,[17] particularly in the case of elements that scatter weakly.[18] The ability to (i) isolate Fe(III) polymers free of crystalline Fe(III) phases and (ii) characterize their structure using techniques that have enhanced spatial resolution relative to EXAFS spectroscopy and are sensitive to the entire atomic network of the polymer would enable a complete description of the structure and reactivity of this Fe(III) phase.

We previously demonstrated that electrocoagulation (EC) using Fe(0) electrodes is well-suited to generate Fe phases with high control of chemical composition.[12] In EC, the controlled production of Fe(II) occurs via an external current applied to an Fe(0) anode, which allows for precise command on the kinetics of Fe(III) formation and ensures negligible build-up of aqueous Fe(II). In addition, by replicating the gradual transport and oxidation of Fe(II) at natural redox boundaries, this method enables us to quantify oxyanion uptake and iron polymerization as a function of time and Fe(II) flux.

In the current study, we aim to (i) isolate bivalent cation and oxyanion-rich Fe(III) polymers and (ii) determine the Fe(III) polymer structure and bonding environments of Ca, As(V), and P ions. To achieve these objectives, we apply EC to chemically varied electrolytes at oxyanion:Fe ratios ranging from 0.1−1.0. We examine As(V)+Ca and P+Ca binary electrolytes, but focus on As(V) because arsenic is a major environmental and public health concern and its large X-ray scattering cross-section make As(V) more suitable than P for X-ray based spectroscopic investigations. We develop a structural model and elucidate the formation pathways for bivalent cation and oxyanion-rich Fe(III) polymers by integrating the results from time-dependent As:Fe and P:Fe solids ratio measurements, sequential ion extractions, As K-edge EXAFS spectroscopy, and the atomic pair distribution function (PDF). The PDF technique provides direct interatomic distances, increased spatial resolution relative to EXAFS spectroscopy, and concurrent detection of the bonding environments of elements that scatter weakly (Ca, P) and strongly (Fe, As). Furthermore, because the PDF technique is sensitive to atomic pairs beyond the first few coordination spheres, this method queries the complete coherent atomic arrangement of short-ranged polymers, thus providing a new view of the Fe(III) polymer phase isolated in our study.

## MATERIALS AND METHODS

**Electrocoagulation Experiments.** Two series of electrolyte solutions were prepared for batch EC experiments: (i) a range of Ca concentrations (330−2000 $\mu$M) in the presence of 150 or 500 $\mu$M As(V), and (ii) a range of As(V) or P (50−500 $\mu$M) in the presence or absence of 1000 $\mu$M Ca. The samples are identified by the initial concentrations of the oxyanion ($\mu$M) and bivalent cation, if present, in the electrolyte. In the subset of experiments in which the Ca concentration was varied, we list the Ca concentration ($\mu$M); however, unless otherwise noted, the concentration of Ca was 1000 $\mu$M. For example, As500+Ca represents an electrolyte that contains initially 500 $\mu$M As(V) and 1000 $\mu$M Ca, whereas As150+Ca330 contains 150 $\mu$M As(V) and 330 $\mu$M Ca. In the absence of Ca, 2 mM NaCl was added to ensure that charge could be passed through the Fe(0) electrode reliably without exceeding the maximum cell voltage allowed by the power supply.

A detailed description of the EC cell configuration and experimental conditions is given in the Supporting Information and was reported previously.[12,19,20] Briefly, in each experiment, 0.5 mM Fe (27.5 mg Fe/L) was produced via Fe(0) electrolysis in a 200 mL volume at an Fe dosage rate of 50 $\mu$M/min, corresponding to a 10 min electrolysis time, with a current density of 2.75 mA/cm$^2$. The Fe dosage rate of 50 $\mu$M Fe/min was selected to ensure that dissolved oxygen did not deplete and Fe(II) did not accumulate in the reactor. In addition, this Fe dosage rate is within the range we investigated previously, where we showed that the structure and arsenic uptake mechanism of Fe(III) precipitates generated in synthetic groundwater were identical at Fe dosage rates ranging from 0.9−287 $\mu$M Fe/min.[20] Following the electrolysis stage, the Fe(0) electrodes were removed, and the suspension reacted for 2 h under continuous stirring with the reactor open to the atmosphere. Throughout the electrolysis and reaction stages, the pH was maintained at 7.5 ± 0.3 using 0.1 M HCl or NaOH.

**Progression of Oxyanion:Fe Solids Ratios with Time.** Oxyanion uptake was measured on a subset of samples by removing and filtering 5 mL aliquots of suspension at 2, 4, 7, and 10 min throughout electrolysis. These time points correspond to Fe additions of 0.1, 0.2, 0.35, and 0.5 mM, or 20, 40, 70, and 100% of the total Fe generated. Samples were also taken at 10, 30, 60, 90, and 120 min after the 10 min electrolysis stage. We calculated the solids ratios of the precipitates generated at each 2−3 min interval by subtracting the aqueous oxyanion concentration measured at the beginning and end of each interval and normalizing by the amount of Fe added during the interval (i.e., $As{:}Fe_{4-7} = ([As(V)]_{aq,4min} - [As(V)]_{aq,7min})/0.15$ mM Fe). No significant amount of Fe was measured in the filtered solution. All experimental conditions were identical to those of the batch experiments.

**Extraction Experiments.** The fractions of As(V)/P, Ca, and Fe mobilized from the solid phase by different reagents were determined by a modified Tessier sequential extraction protocol.[21] Rather than submerging the filtered solids (5 mg Fe per batch experiment) into the extraction solutions, the solids were left on a filter membrane, and the extractants were flushed through the filter membrane at a rate of 1−3 mL/min before submerging the filter into oxalic acid in the final step. First, deionized (DI) water was flushed to target any entrained solution and/or ions unassociated with the particles. Second, a 1.0 M NaCl solution was flushed to target weakly sorbed ions easily displaced by high ionic strength or by high concentrations of non-interacting solutes. Finally, to target the strongly sorbed ions, filtered material was digested in 0.1 M oxalic acid at pH 3.3. A 10 mL volume was selected for each extraction step and for the final digestion. In preliminary extraction experiments, we flushed the filtered solids with two sequential 10 mL volumes and found that the ion concentrations in the second 10 mL flush were typically less than 10% of those in the first flush. The fractions of As(V), P, Ca, and Fe mobilized by DI water, NaCl, and oxalic acid were calculated by normalizing the total amount of each ion extracted in each step by the total recovered from all three steps.

**Synchrotron-Based X-ray Characterization.** High-energy X-ray scattering data suitable for PDF analysis were obtained from reference minerals (see Supporting Information for synthesis procedures) and experimental samples at beam line 11 ID-B of the Advanced Photon Source (APS) at Argonne National Laboratory (ANL; Argonne, IL). Data were collected on an amorphous Si image-plate detector (General Electric) [22]

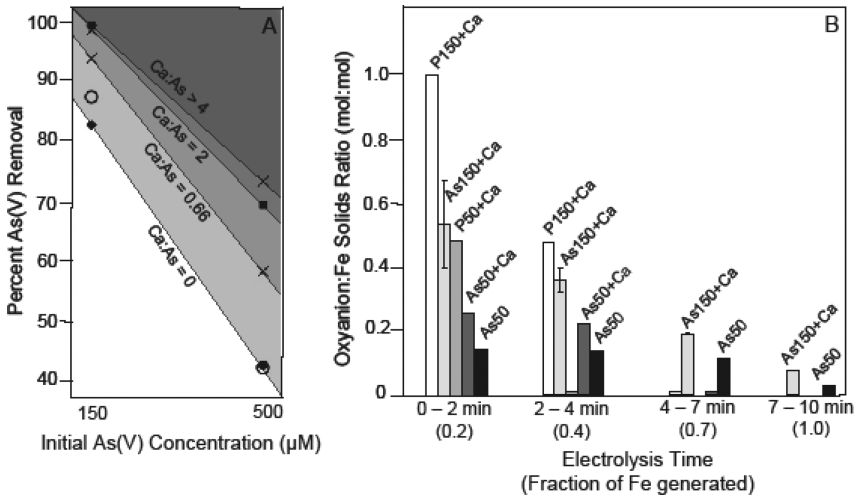


**Figure 1.** (A) Percent removal of 150 and 500 $\mu$M As(V) after 2 h reaction time in batch experiments with an input of 500 $\mu$M Fe at increasing initial Ca:As molar ratios from 0 to >4. The filled diamonds and squares represent the samples with initial Ca concentrations of 0 and 1000 $\mu$M, respectively, whereas the crosses and diagonal shaded regions demarcate increasing initial Ca concentrations ranging from 100−2000 $\mu$M. The open circles show the percent As(V) removal when 1000 $\mu$M Ca was added 30 min after the electrolysis stage. (B) Oxyanion:Fe solids ratio (mol:mol) of precipitates generated at different stages of electrolysis. Initial oxyanion concentrations in units of $\mu$M are indicated in the sample name. All of the data are reported as the average of replicate experiments. Error bars, if present, indicate the standard deviation of the triplicate measurements.

**Table 1. As(V) Removal As a Function of Initial Ca Concentration**

| Sample | Initial Value ($\mu$M) | | Initial Ratio (mol:mol) | | Percent Removal | | Average Solids Ratio (mol:mol) | |
|---|---|---|---|---|---|---|---|---|
| | As | Ca | As:Fe | Ca:As | As | SD[a] | As:Fe | SD[a] |
| As150 | 150 | | 0.3 | 0 | 82 | 9.2 | 0.25 | 0.03 |
| As150 + 100Ca | 150 | 100 | 0.3 | 0.66 | 93 | | 0.28 | |
| As150 + 300Ca | 150 | 300 | 0.3 | 2.0 | 98 | | 0.29 | |
| As150 + 1000Ca | 150 | 1000 | 0.3 | 6.6 | 99 | 0.7 | 0.30 | <0.01 |
| As150 + 30min + 1000Ca | 150 | 1000 + 30 min | 0.3 | 0 | 87 | | 0.26 | |
| As500 | 500 | | 1.0 | 0 | 42 | 7.1 | 0.42 | 0.07 |
| As500 + 330Ca | 500 | 330 | 1.0 | 0.66 | 58 | | 0.58 | |
| As500 + 1000Ca | 500 | 1000 | 1.0 | 2.0 | 69 | 4.1 | 0.69 | 0.04 |
| As500 + 2000Ca | 500 | 2000 | 1.0 | 4.0 | 73 | | 0.73 | |
| As500 + 30min + 1000Ca | 500 | 1000 + 30 min | 1.0 | 0 | 42 | | 0.42 | |
| As1000 + 1000Ca | 1000 | 1000 | 2.0 | 1.0 | 41 | | 0.82 | |

[a]The standard deviation is given for the experiments done at least in triplicate.

out to a $Q$-value near 29 Å$^{-1}$ at room temperature using 58.9 keV ($\lambda$ = 0.2128 Å) X-rays. The total structure function, $S(Q)$, and the PDF, $G(r)$, were obtained using the program PDFgetX2 [23] using standard correction procedures, including those to correct for the image-plate geometry.[22] Our reference mineral refinements and our procedures to obtain the partial component PDFs of reference minerals and difference PDFs (d-PDFs) of samples are described in detail in the Supporting Information. X-ray absorption spectra at the As K-edge were acquired at beam lines 11−2 (fluorescence) and 4−1 (fluorescence and transmission) of the Stanford Synchrotron Radiation Lightsource (SSRL; Menlo Park, CA) under typical ring conditions of 350 mA at 3.0 GeV. The curve fittings were carried out in $R$ + $\Delta R$-space (Å) using the SixPack software, which is built on algorithms derived from the IFEFFIT library.[24] Detailed descriptions of our As K-edge EXAFS shell-by-shell fitting procedure appear in the Supporting Information.

## RESULTS AND DISCUSSION

**As(V) Uptake by Fe(III) Precipitates at Varying Initial Ca Concentrations.** Figure 1, panel A and Table 1 show the percent As(V) removal in samples where the initial Ca:As molar ratio varied from 0−6.6 with an input of 500 $\mu$M Fe. An increase in the initial Ca:As ratio from 0−0.66 enhanced the removal of As(V) by approximately 9 and 16% in samples with 150 and 500 $\mu$M initial As(V), respectively. Greater As(V) removal was observed for an initial Ca:As ratio of 2, but no further As(V) removal was observed at Ca:As ratios greater than 2 (Table 1).

The removal of As(V) when 1000 $\mu$M Ca was added 30 min after the end of electrolysis is indicated in Figure 1, panel A. At an initial As(V) concentration of 150 $\mu$M, the addition of Ca 30 min after electrolysis increased As(V) removal by approximately 5% compared to the 9% increase in As(V) removal when an order of magnitude less Ca was added before electrolysis (100 $\mu$M Ca, Ca:As = 0.66). Thus, the Ca added 30 min after electrolysis, that is, after all of the Fe had polymerized, was only half as effective at enhancing As(V) removal as a much lower Ca concentration present at the start of Fe(III) nucleation. Furthermore, at 500 $\mu$M initial As(V), the addition of Ca after electrolysis (1000 $\mu$M Ca, Ca:As = 2.0) had a negligible impact on As(V) removal, whereas Ca present prior

Table 2. Sample Solids Ratios and Ion Extractions[a]

| Sample | Solids Ratio (mol:mol) | | | Extracted Ca (%) | | | Oxalic Acid Extracted Ratio (mol:mol) | | |
|---|---|---|---|---|---|---|---|---|---|
| | As:Fe | P:Fe | Ca:Fe | DI | NaCl | oxalic acid | As/P:Fe | Ca:Fe | Ca:As/P |
| As50 | 0.10 | | | | | | 0.10 | | |
| As50+Ca | 0.10 | | 0.15 | 21 | 63 | 17 | 0.09 | 0.01 | 0.09 |
| As150 | 0.25 | | | | | | 0.24 | | |
| As150+Ca | 0.30 | | 0.19 | 11 | 71 | 17 | 0.28 | 0.02 | 0.06 |
| As500 | 0.42 | | | | | | 0.41 | | |
| As500+Ca | 0.69 | | 0.40 | 3 | 73 | 25 | 0.63 | 0.05 | 0.08 |
| P500+Ca | | 0.94 | 0.70 | 1 | 31 | 68 | 0.97 | 0.40 | 0.41 |

[a]Reported values represent the average of replicate experiments. The mobilized fractions of Fe, As(V), and Ca varied by < 0.1 in replicate experiments.

to electrolysis enhanced As(V) removal by 16% (330 $\mu$M Ca; Ca:As = 0.66). These results indicate that Ca impacts As(V) uptake most significantly at the onset of Fe(III) precipitation when Ca can enhance As(V) removal by modifying the structure of the nascent Fe(III) precipitate.

**Progression of Oxyanion:Fe Solids Ratios with Time.** Figure 1, panel B shows the average oxyanion:Fe solid ratios calculated for the Fe(III) precipitates generated during each 2−3 min interval over the 10 min period when Fe(II) was dosed into solution via Fe(0) electrolysis. Tabulated concentrations of aqueous As(V) and P appear in Table SI1 of the Supporting Information. In the As50 sample (50 $\mu$M initial As(V)), the moderate As:Fe solids ratio achieved at each time interval did not deplete aqueous As(V) until all Fe had been dosed into solution. Similarly, As(V) remained in solution throughout the electrolysis stage in the As150+Ca sample. These results show that in As50 and As150+Ca samples, the majority of Fe polymerizes in the presence of aqueous As(V), which is known to disrupt Fe−Fe bonding and promote the formation of disordered Fe phases. Conversely, the large As:Fe or P:Fe solids ratios in the precipitates formed at the onset of electrolysis in the As50+Ca, P50+Ca, and P150+Ca samples depleted rapidly all As(V) and P from solution (Table SI1, Supporting Information). In these samples, the electrolyte contained no measurable oxyanion 4 min after the onset of electrolysis. Consequently, all Fe added to the system during the last 6 min of electrolysis polymerized to form more crystalline Fe phases with oxyanion:Fe solids ratios near 0. These data are consistent with the sequential formation of multiple solid phases:[4,10] a disordered, polymeric Fe(III) precipitate with a large oxyanion sorption capacity forms at the onset of electrolysis followed by a more crystalline Fe(III) (oxyhydr)oxide after aqueous oxyanions are removed from solution. This conclusion is supported by transmission electron micrographs of the As50+Ca sample, which display two distinct morphologies (Figure SI1, Supporting Information): a needle-like platelet consistent with the morphology of lepidocrocite interspersed throughout rounded, semispherical aggregates lacking crystallinity.

In the P150+Ca sample, the precipitates formed in the first 2 min of electrolysis (Figure 1B) had P:Fe solids ratios near 1.0. The solids ratio achieved in this time interval is similar to that of the P500+Ca sample averaged over the entire 10 min electrolysis stage. By contrast, the P:Fe solids ratio in the P50+Ca sample averaged over the first 2 min was 0.5. This solids ratio corresponds to the value expected if the precipitates generated during the first minute of electrolysis have a P:Fe solids ratio of 1.0 and the precipitates generated in the second minute have a P:Fe solids ratio of 0. To confirm that a P-rich phase with a P:Fe solids ratio near 1.0 formed during the first minute of electrolysis in the P50+Ca sample, we measured P uptake after 1 min. In fact, we found that aqueous P was nearly depleted after 1 min and that the Fe(III) phase achieved a P:Fe solids ratio of 0.9. These results provide compelling evidence that the formation of oxyanion-rich Fe(III) polymers is controlled by the oxyanion:Fe solution ratio at the time of polymerization, rather than the initial oxyanion concentration. However, the accumulation of the polymer as a single phase depends both on the ratio of initial oxyanion concentration to the amount of Fe dosed and the presence of Ca. Because the P500+Ca sample has an average P:Fe solids ratio near 1.0 (Table 2), which is similar to the solids ratios of the precipitates formed initially in the P50+Ca and P150+Ca samples, we use the P500+Ca sample to infer the structure of the Fe(III) polymers formed at the onset of electrolysis at lower oxyanion concentrations. Although the initial 500 $\mu$M As(V)/P concentrations of the As500+Ca and P500+Ca samples may be larger than typical environmental concentrations, these single-phase samples permit structural characterization of the polymers contained in the multiphase solids that are generated at the lower, more environmentally relevant oxyanion concentrations in our study.

**Ion Extraction.** Table 2 and Figure SI2 of the Supporting Information show the fractions of As(V), P, and Ca extracted from the Fe(III) precipitates by 18 MΩ DI water, 1.0 M NaCl, and oxalic acid at pH 3.3. In all samples, nearly 100% of the mobilized As(V), P, and Fe was extracted in the oxalic acid digestion. Thus, the oxalic acid-extracted As:Fe and P:Fe ratios were similar to the average solids ratios measured in the batch experiments. These results indicate that mobilization of oxyanions requires the dissolution of the solid Fe(III) phase. This strong coupling between the mobilized Fe and As(V)/P is consistent with direct bonding between As(V)/P and the Fe(III) precipitates.[7,14]

The mobilization of Ca, unlike that of As(V) and P, occurred in both the NaCl and oxalic acid steps. Because NaCl extraction mobilized Ca without a significant quantity of oxyanions, we rule out that any proportion of As(V) or P could be bound in weakly sorbed Ca-As(V)/P ion pairs or in outer-sphere complexes. The fraction of Ca released in the oxalic acid step increased in the order of As50+Ca < As150+Ca < As500+Ca < P500+Ca, which follows the same order of increasing Ca uptake observed in the batch experiments (Table 2). These trends are consistent with the formation of oxyanion−Ca bonds; however, the dominant oxyanion−Ca bonding mode appears to differ in the As(V)+Ca and P+Ca systems. In the As500+Ca sample, the NaCl extraction released more than 70% of the mobilized Ca, which suggests that the majority of Ca is

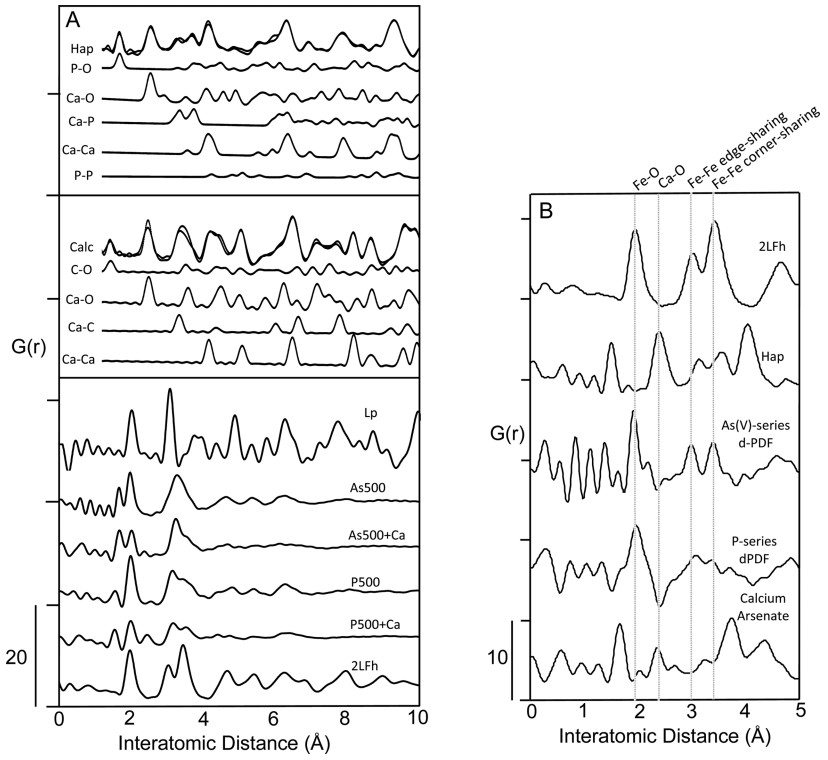


**Figure 2.** Top two panels in A show the Hap and Calc PDF refinements overlain to the experimental data. The partial component PDFs derived from the refined PDF are presented below each complete refinement. The bottom panel in A shows the PDFs of the As500, As500+Ca, P500, and P500+Ca samples along with the PDFs of the reference minerals lepidocrocite (Lp) and 2-line ferrihydrite (2LFh). In panel B, the d-PDFs of the experimental PDFs in the bottom panel of A are compared to the PDFs of 2LFh and calcium arsenate. The vertical lines shown in B highlight peaks due to characteristic interatomic pairs.

most likely associated with the particles via electrostatic interactions. In contrast, the oxalic acid digestion released nearly 70% of the mobilized Ca in the P500+Ca sample, which suggests significant Ca−P−Fe ternary interactions or the formation of a discreet Ca−P phase. However, we argue against the formation of Ca−P solid in a subsequent section.

The Ca:As:Fe and Ca:P:Fe ratios obtained from the oxalic-acid digestions provide a measure of the stoichiometry of As(V)/P and Ca strongly associated with the solid phase. The oxalic acid-mobilized Ca:As ratios for all samples in the As(V)+Ca series are near 0.1, which suggests that strongly sorbed Ca comprises a small fraction of the overall solid phase. In the P500+Ca sample, Ca and P are mobilized at a ratio of nearly 0.4 Ca:P, which is consistent with a polymer containing a Ca:P:Fe stoichiometry of 0.4:1:1.

**Polyhedral Linkages in Reference Minerals.** To interpret the short- to intermediate-ranged atomic configurations in the samples, we first examine the PDFs of a suite of reference minerals, where the PDF can be interpreted as a histogram of interatomic distances within the coherently scattering structure. The PDF refinements of hydroxyapatite (Hap; $Ca_5(PO_4)_3OH(s)$) and calcite (Calc; $CaCO_3(s)$) are overlain to the measured PDFs in the top sections of Figure 2, panel A, with the partial component PDFs shown below each complete refinement. A summary of the refinement results for all of the reference minerals is given in Table SI2 of the Supporting Information.

For hydroxyapatite, the first four peaks in the PDF at 1.5, 2.4, 3.2, and 3.6 Å are due to P−O, Ca−O, P−Ca, and P−Ca linkages, respectively. The Ca and P polyhedra that produce these peaks are bound together by single corner-sharing linkages, with the two different Ca−P distances due to highly distorted Ca polyhedra.[25] The next peak in hydroxyapatite occurs near 4.0 Å and reflects major contributions from Ca−Ca atomic pairs and, to a lesser extent, Ca−O atomic pairs. For Calc, the PDF shows a C−O peak near 1.3 Å and a Ca−O peak near 2.3−2.4 Å. The next major feature near 3.3 Å is due to a combination of Ca−O and Ca−C atomic pairs. The first peak due to Ca−Ca pairs in the Calc PDF appears near 4.0 Å, which together with a Ca−O peak near 4.4 Å contributes to the split peak from 3.8−4.5 Å. The PDF refinements of other reference minerals, including lepidocrocite ($\gamma$-FeOOH(s)), and 2-line ferrihydrite, along with a description of the characteristic peaks in these reference minerals, are discussed by van Genuchten et al.[12]

**Pair Distribution Functions of Fe(III) Polymers.** The bottom section in Figure 2, panel A presents the PDFs of the As500+Ca and P500+Ca samples together with the PDFs of the As500 and P500 samples in order to compare the effects of Ca on the solid phase structure. Relative to the As500+Ca PDF, the As500 PDF contains better resolved peaks of larger amplitude in the region from 4−7 Å, which indicates greater Fe−Fe polymerization.[12] To examine further the structural differences between the As500 and As500+Ca samples, we compared the d-PDF of these samples and the analogous P-series d-PDF to the PDFs of reference minerals in Figure 2, panel B. The negative peak in the As500−(As500+Ca) d-PDF near 2.4 Å is consistent with the position of the Ca−O peak in the hydroxyapatite and calcium arsenate PDFs, which confirms the presence of Ca in the As500+Ca sample. In addition, two well-resolved peaks consistent with edge- and corner-sharing Fe(III) polyhedra emerge in the region from 3.0−3.4 Å. The

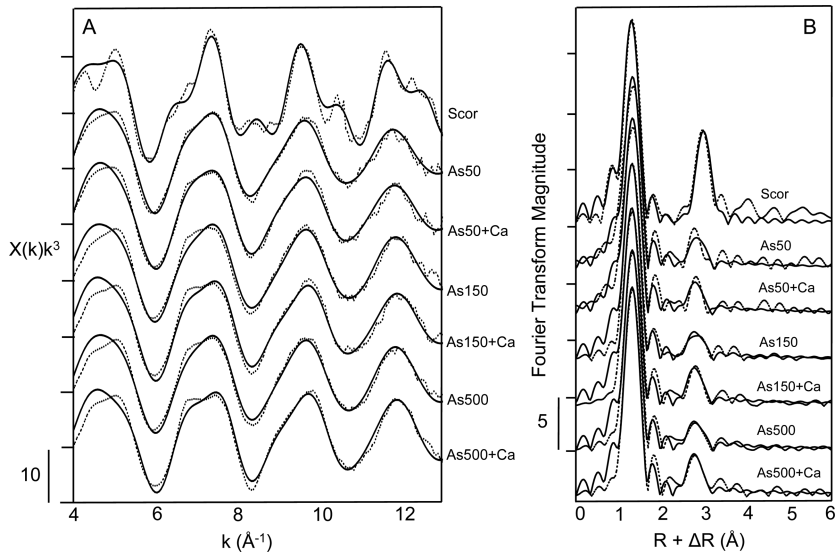


**Figure 3.** (A) As K-edge EXAFS spectra and (B) Fourier-transformed As K-edge EXAFS spectra of scorodite (Scor) and the experimental samples in the As and As+Ca concentration series. The outputs of the shell-by-shell fits (solid lines) are overlain on the data (dotted lines).

presence of these two peaks in the As500−(As500+Ca) d-PDF, combined with (i) the increased amplitude in the 4−7 Å region, (ii) the larger coherent scattering domain, and (iii) the lower As:Fe solids ratio of the As500 sample relative to the As500+Ca sample indicates greater edge and corner-sharing Fe−Fe polyhedral connectivity in the As500 sample than in the As500+Ca sample. Although the atomic pairs from Ca−O were resolved in this d-PDF, it was not possible to resolve peaks due to Ca−As atomic pairs, which is consistent with the minor fraction of oxalic acid-extracted Ca.

The P-series PDFs presented in Figure 2, panel A contain peaks near 1.6, 2.0, and 3.2 Å due to P−O, Fe−O and P−Fe scattering, respectively. The peaks in the P500 PDF in the region from 4−7 Å are due to edge- and corner-sharing Fe polyhedra and resemble those of the As500 PDF, which is in agreement with their similar oxyanion:Fe solids ratios. Similar to the As500+Ca PDF, the P500+Ca PDF contains no major features beyond 4 Å, which reflects the polymeric nature of the samples containing high P:Fe or As:Fe solids ratios. Consistent with the largest Ca:Fe solids ratio of any sample, the P500+Ca PDF contains a Ca−O peak near 2.4 Å, which is confirmed in the d-PDF (Figure 2, panel B). Beyond the first P−O, Fe−O, Ca−O, and P−Fe correlations, a new peak in the P500+Ca PDF is resolved with a maximum near 3.6 Å; this peak is not visible in the PDF of any other sample. The position of this peak is consistent with the Ca−P peak near 3.6 Å in hydroxyapatite, which is due to direct Ca−P bonding. Consequently, we propose that short-ranged Ca−P bonds form in the Fe(III)−P−Ca polymer with Ca bonded to P in a hydroxyapatite-like corner-sharing configuration. This interpretation is supported by the larger quantity of oxalic-acid extracted Ca in this sample, which is more likely to scatter coherently beyond the first Ca−O shell than the weakly sorbed Ca. The formation of a distinct Ca−P mineral in the P500+Ca sample is not supported by the PDF, which shows only broad atomic pair correlations beyond 4 Å and none beyond 7 Å, and thus a negligible contribution beyond the second-nearest neighbor atomic pairs. The peak near 3.6 Å could be interpreted as evidence for mononuclear corner-sharing Fe−Fe linkages;[14] however, we argue against this because (i) P is well-known to inhibit corner-sharing Fe polyhedra, (ii) the absence of significant pair correlations beyond 4 Å shows that Fe−Fe polymerization is extremely limited in this sample, and (iii) this peak appears only in the P500+Ca sample, which contains strongly sorbed Ca with a 0.4:1:1 Ca:P:Fe stoichiometry.

**As(V) Coordination Environment.** The As K-edge EXAFS spectra and Fourier transforms (uncorrected for phase-shift) from a subset of samples and reference minerals are overlain to the shell-by-shell fitting output in Figure 3. A summary of the fit results appears in Table SI3 of the Supporting Information. Fits of the first shell for all samples and reference minerals returned values near 4 for $N_{As-O}$ and 1.68−1.70 Å for $R_{As-O}$, which confirms the tetrahedral coordination of As(V). The second-shell fit of scorodite resulted in values of 3.4 ± 1.0 for $N_{As-Fe}$ and 3.35 ± 0.01 Å for $R_{As-Fe}$, which are in excellent agreement with crystallographic values.[26] The second-shell fits of all experimental samples are within the fit derived uncertainties of an As−Fe path with $R_{As-Fe}$ of 3.28 Å and $N_{As-Fe}$ of 2. These structural parameters are consistent with $AsO_4$ tetrahedra bound to Fe(III) polyhedra in the binuclear, corner-sharing ($^2$C) geometry.[7] Attempts to add an additional As−Fe path at 3.6 Å, which correspond to a mononuclear corner-sharing ($^1$C) complex,[7] were not supported by the fit (physically unrealistic fit-derived $\sigma^2$ or $N$). In the samples generated in the presence of Ca, attempts to add an As−Ca path with $R_{As-Ca}$ values of 3.2, 3.4, or 3.6 Å such as those found in the mineral johnbaumite[25] were also not supported by the fit. Thus, As(V) is primarily bound to Fe(III) polyhedra in the same $^2$C geometry regardless of the presence or absence of Ca in the samples.

**Structural Model of Fe(III) Polymers.** In this section, we derive structural models for Fe(III)−As(V)−Ca and Fe(III)−P−Ca polymers based on the batch and time-dependent oxyanion:Fe solids ratio results, extraction data, PDF data, and As K-edge EXAFS spectra. Based on the strong coupling between As and Fe in the extraction data, the intense As−Fe peak near 3.2−3.3 Å in the PDF, and the shell-by-shell fits of the As K-edge EXAFS spectra, we constrain the primary As(V) binding mode to that of the $^2$C geometry where $AsO_4$

tetrahedra bind to apical oxygen atoms of edge-sharing Fe polyhedral dimers and trimers. Following previous work, we consider the formation of the triangular edge-sharing Fe trimers to be more likely than linear trimers.[27,28] The Ca:As ratio in the oxalic acid digestion suggests that direct Ca−As bonding is limited to a Ca:As ratio of approximately 1:10 (i.e., roughly 10% of solid-phase As(V) coordinates directly to Ca), which explains the insignificant contribution of Ca to the second-shell of the As K-edge EXAFS spectra. Although we expect Ca to favor bonding to sorbed As(V) tetrahedra rather than to Fe(III) based on our chemical extractions and the chemical similarity between As(V) and P, our As K-edge EXAFS spectra and PDF data do not allow us to rule out a minor fraction of Ca sorbed directly to Fe(III) polyhedra. An additional constraint on the coherent arrangement of Ca, As, and Fe atoms in the As500+Ca sample is provided by the less than 7 Å coherent scattering domain observed in the PDF. Based on these chemical and structural data, we suggest the structural model in Figure 4, panel A, where Ca adopts two bonding environments: (i) "structural" Ca that is coordinated directly to sorbed As(V) and (ii) "extractable" Ca that is associated with the solid in weakly sorbed configurations. Both the extraction experiments and synchrotron-based characterization data indicate that the fraction of structural Ca in the Fe(III)−As(V)−Ca polymers is small relative to extractable Ca.

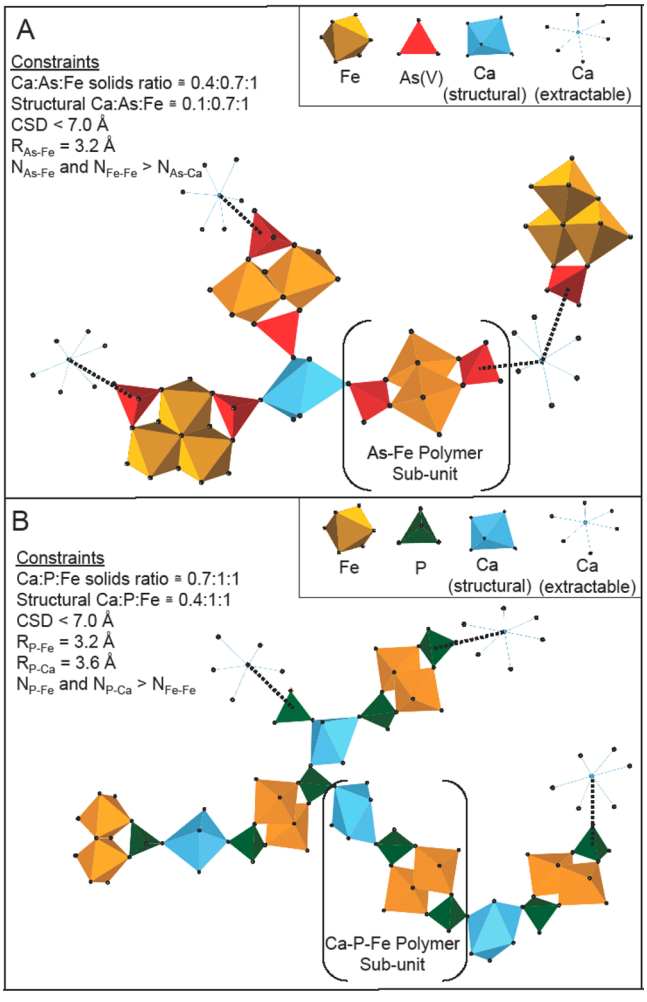


**Figure 4.** Visual representation of the models derived for (A) Fe(III)−As(V)−Ca and (B) Fe(III)−P−Ca polymers that form at the onset of Fe(III) precipitation in the presence of Ca and As(V) or P.

In the P500+Ca sample, the oxalic acid digestion suggests the formation of a polymer with a Ca:P:Fe stoichiometry close to 0.4:1:1. Based on the PDF, the coherent scattering domain in the Fe(III)−P−Ca polymer is less than 7 Å and P−Fe and P−Ca linkages occur at 3.2 and 3.6 Å, respectively. In Figure 4, panel B, we present a structural model based on these chemical and structural data. In agreement with the larger oxyanion:Fe solids ratio in the P500+Ca sample (P:Fe = 1.0) relative to that of the As500+Ca sample (As:Fe = 0.7), the P-series contains more structural Ca, which is expected to enhance oxyanion uptake more effectively than extractable Ca. Although the coherently scattering atoms in this polymer are limited to the 7 Å Ca−O−P−$(O-Fe)_2$ subunit, any incoherent scattering that arises from intercrystallite aggregation would not be detected by the PDF technique. Aggregation processes, however, govern macroscopic particle size and explain why poorly ordered crystallites, including the polymers isolated in our study, can be easily separated from solution.[12]

The formation of ternary Fe−As(V)/P−Ca sorption complexes is debated in the surface complexation modeling literature,[13,29−31] and direct spectroscopic evidence of these configurations is scarce.[4,32] In the polymer structural models shown in Figure 4, we propose that Ca bonds indirectly and directly to As(V)/P oxyanions sorbed to Fe(III) polyhedra. The direct detection of oxyanion−Ca bonds was only possible in the P+Ca system, which is reflected in our models by the relatively minor fraction of Fe−As(V)−Ca ternary configurations. Thus, our interpretation of ternary complexes involving Ca is more speculative in the As(V)+Ca system relative to the P+Ca system. The atomic arrangement of Fe, As(V)/P, and Ca in our structural models is expected to extend beyond polymers and molecular clusters. These models are likely representative of complex bonding environments at mineral surfaces.[33,34]

**Environmental Implications.** In this work, we propose that Fe(II) oxidation and Fe(III) polymerization in the presence of Ca and As(V)/P leads to the formation of a polymeric Fe(III) phase that consists of a less than 7 Å coherent network of corner-sharing As(V)/P tetrahedra coordinated to Fe(III) polyhedra, with varying amounts of Ca sorbed to the oxyanion. This phase forms at the onset of Fe(II) oxidation in the presence of oxyanions and bivalent cations and achieves large oxyanion:Fe solids ratios. The formation of a polymer phase with an oxyanion:Fe stoichiometry of 0.7−1.0 suggests that only a small amount of Fe is required to deplete the aqueous phase of any oxyanion. Fe(III) generated after the depletion of oxyanions forms lepidocrocite. Although the flux of Fe(II) and the initial oxyanion concentrations may be lower in natural systems than in our study, we show that the formation of the oxyanion-rich polymer is governed by the oxyanion:Fe ratio in solution during Fe(III) polymerization. At natural redox boundaries in groundwater and soils where Fe(II) is oxidized in the presence of bivalent cations and oxyanions, we expect that oxyanion-rich polymers can form, but their accumulation (and thus detection) requires initial oxyanion:Fe molar ratios larger than 1.0. At lower oxyanion:Fe concentrations, the formation of more crystalline minerals after the depletion of oxyanions can mask the polymer phase when present as a moderate fraction of the total Fe(III) solids due to its X-ray transparent nature. Nonetheless, these oxyanion-rich Fe(III) polymers must be

accounted for when assessing the Fe(III) phase that controls oxyanion mobility at natural redox boundaries.

The subnanoscale crystallite size of oxyanion-rich Fe(III) polymers renders current models of nanoparticulate Fe(III) precipitates, such as 2-line ferrihydrite, inadequate to predict their reactivity. The Fe(III) polymers described in this study exhibit higher oxyanion:Fe solids ratios and significantly lower crystallite sizes than 2-line ferrihydrite, which suggests that the chemical or biologically mediated turnover of these Fe(III) phases, and the concomitant release of sorbed ions, may be faster than that of more crystalline Fe oxides. For example, Hyacinthe and Van Capellen[9] found that ascorbate induced the reductive dissolution of more than 97% of a P-rich Fe(III) phase after 24 h, whereas less than 3−25% of crystalline lepidocrocite and hematite dissolved in the same time period. This result is corroborated by the time scale of Fe(III) dissolution observed in our experiments. We found that dissolution by oxalic acid in samples containing lepidocrocite required approximately two orders of magnitude longer times than did the single-phase Fe(III) polymers. Consequently, the highly reactive and dynamic pool of Fe contained in these polymeric phases may play a key role in the fate of trace and major elements and the chemical and microbial-induced cycling of Fe in natural and engineered systems.

## ■ ASSOCIATED CONTENT

### Supporting Information

Detailed descriptions of the EC cell configuration and operating parameters; the syntheses of reference minerals; and the data collection, reduction, and analysis of high energy X-ray scattering data and EXAFS spectra. TEM images and tabulated measurements of aqueous As(V) and P as a function of time. This material is available free of charge via the Internet at http://pubs.acs.org.

## ■ AUTHOR INFORMATION

### Corresponding Author

*Phone: +1 (510) 664-4343; e-mail: cmvangenuchten@berkeley.edu.

### Present Address

[⊥]C.M.vG., Institut de Dynamiques de la Surface Terrestre, University of Lausanne, Lausanne, Switzerland.

### Notes

The authors declare no competing financial interest.

## ■ ACKNOWLEDGMENTS

We thank the Associate Editor and reviewers of our manuscript for their helpful comments that improved this work. We gratefully acknowledge the following researchers for their technical assistance and advice along the various stages of this work: Amanda Finger, Caroline Delaire, Sharon Bone, Jeff Maske, Erik Nelson, Kevin Beyer, Karena Chapman, F. Marc Michel, and Garrison Sposito. This work was supported by a National Science Foundation Graduate Research Fellowship to C.M.vG. We acknowledge support from the Herbette Foundation (University of Lausanne), the Richard C. Blum Center for Developing Economies (University of California, Berkeley), and the Sandoz Family Foundation for the support of this research. Portions of this research were carried out at the Stanford Synchrotron Radiation Lightsource, a Directorate of SLAC National Accelerator Laboratory and an Office of Science User Facility operated for the U.S. Department of Energy (DOE) Office of Science by Stanford University. Use of the Advanced Photon Source, an Office of Science User Facility operated for the U.S. DOE Office of Science by Argonne National Laboratory, was supported by the U.S. DOE under Contract No. DE-AC02-06CH11357.

## ■ REFERENCES

(1) Buffle, J.; Devitre, R.; Perret, D.; Leppard, G. Physicochemical characteristics of a colloidal iron phosphate species formed at the oxic−anoxic interface of a eutrophic lake. *Geochim. Cosmochim. Acta* **1989**, *53* (2), 399−408.

(2) Gunnars, A.; Blomqvist, S.; Johansson, P.; Andersson, C. Formation of Fe(III) oxyhydroxide colloids in freshwater and brackish seawater, with incorporation of phosphate and calcium. *Geochim. Cosmochim. Acta* **2002**, *66* (5), 745−758.

(3) Perret, D.; Gaillard, J.; Dominik, J.; Atteia, O. The diversity of natural hydrous iron oxides. *Environ. Sci. Technol.* **2000**, *34* (17), 3540−3546.

(4) Voegelin, A.; Kaegi, R.; Frommer, J.; Vantelon, D.; Hug, S. J. Effect of phosphate, silicate, and Ca on Fe(III)-precipitates formed in aerated Fe(II)- and As(III)-containing water studied by X-ray absorption spectroscopy. *Geochim. Cosmochim. Acta* **2010**, *74* (1), 164−186.

(5) Rancourt, D.; Fortin, D.; Pichler, T.; Thibault, P.; Lamarche, G.; Morris, R.; Mercier, P. Mineralogy of a natural As-rich hydrous ferric oxide coprecipitate formed by mixing of hydrothermal fluid and seawater: Implications regarding surface complexation and color banding in ferrihydrite deposits. *Am. Mineral.* **2001**, *86* (7−8), 834−851.

(6) Majzlan, J.; Lalinska, B.; Chovan, M.; Jurkovic, L.; Milovska, S.; Gottlicher, J. The formation, structure, and ageing of As-rich hydrous ferric oxide at the abandoned Sb deposit Pezinok (Slovakia). *Geochim. Cosmochim. Acta* **2007**, *71* (17), 4206−4220.

(7) Waychunas, G. A.; Rea, B. A.; Fuller, C. C.; Davis, J. A. Surface-chemistry of ferrihydrite 0.1. EXAFS studies of the geometry of coprecipitated and adsorbed arsenate. *Geochim. Cosmochim. Acta* **1993**, *57* (10), 2251−2269.

(8) Hyacinthe, C.; Bonneville, S.; Van Cappellen, P. Reactive iron(III) in sediments: Chemical versus microbial extractions. *Geochim. Cosmochim. Acta* **2006**, *70* (16), 4166−4180.

(9) Hyacinthe, C.; Van Cappellen, P. An authigenic iron phosphate phase in estuarine sediments: Composition, formation, and chemical reactivity. *Mar. Chem.* **2004**, *91* (1−4), 227−251.

(10) Voegelin, A.; Senn, A.; Kaegi, R.; Hug, S.; Mangold, S. Dynamic Fe-precipitate formation induced by Fe(II) oxidation in aerated phosphate-containing water. *Geochim. Cosmochim. Acta* **2013**, *117*, 216−231.

(11) Wilkie, J. A.; Hering, J. G. Adsorption of arsenic onto hydrous ferric oxide: Effects of adsorbate/adsorbent ratios and co-occurring solutes. *Colloids Surf., A* **1996**, *107*, 97−110.

(12) van Genuchten, C. M.; Peña, J.; Amrose, S. E.; Gadgil, A. J. Structure of Fe(III) precipitates generated by the electrolytic dissolution of Fe(0) in the presence of groundwater ions. *Geochim. Cosmochim. Acta* **2014**, *127*, 285−304.

(13) Kanematsu, M.; Young, T.; Fukushi, K.; Green, P.; Darby, J. Arsenic(III, V) adsorption on a goethite-based adsorbent in the presence of major co-existing ions: Modeling competitive adsorption consistent with spectroscopic and molecular evidence. *Geochim. Cosmochim. Acta* **2013**, *106*, 404−428.

(14) Rose, J.; Manceau, A.; Bottero, J. Y.; Masion, A.; Garcia, F. Nucleation and growth mechanisms of Fe oxyhydroxide in the presence of $PO_4$ ions 0.1. Fe K-edge EXAFS study. *Langmuir* **1996**, *12* (26), 6701−6707.

(15) Kaegi, R.; Voegelin, A.; Folini, D.; Hug, S. Effect of phosphate, silicate, and Ca on the morphology, structure, and elemental composition of Fe(III)-precipitates formed in aerated Fe(II)- and As(III)-containing water. *Geochim. Cosmochim. Acta* **2010**, *74* (20), 5798−5816.

(16) Baumgartner, J.; Morin, G.; Menguy, N.; Gonzalez, T.; Widdrat, M.; Cosmidis, J.; Faivre, D. Magnetotactic bacteria form magnetite from a phosphate-rich ferric hydroxide via nanometric ferric (oxyhydr)oxide intermediates. *Proc. Natl. Acad. Sci. U. S. A.* **2013**, *110* (37), 14883−14888.
(17) Ravel, B.; Kelly, S. In *The Difficult Chore of Measuring Coordination by EXAFS*; AIP Conference Proceedings: Stanford, CA, 2007; pp 150-152.
(18) Kelly, S. D.; Hesterberg, D.; Ravel, B. Analysis of soils and minerals using X-ray absorption spectroscopy. In *Methods of Soil Analysis. Part 5. Mineralogical Methods*, SSSA Book Series No. 5; Soil Science Society of America: Madison, WI, 2008.
(19) Li, L.; van Genuchten, C. M.; Addy, S. E. A.; Yao, J.; Gao, N.; Gadgil, A. J. Modeling As(III) oxidation and removal with iron electrocoagulation in groundwater. *Environ. Sci. Technol.* **2012**, *46* (21), 12038−12045.
(20) van Genuchten, C.; Addy, S.; Peña, J.; Gadgil, A. Removing arsenic from synthetic groundwater with iron e: An Fe and As K-edge EXAFS Study. *Environ. Sci. Technol.* **2012**, *46* (2), 986−994.
(21) Tessier, A.; Campbell, P.; Bisson, M. Sequential extraction procedure for the speciation of particulate trace-metals. *Anal. Chem.* **1979**, *51* (7), 844−851.
(22) Chupas, P.; Qiu, X.; Hanson, J.; Lee, P.; Grey, C.; Billinge, S. Rapid-acquisition pair distribution function (RA-PDF) analysis. *J. Appl. Crystallogr.* **2003**, *36*, 1342−1347.
(23) Farrow, C.; Juhas, P.; Liu, J.; Bryndin, D.; Bozin, E.; Bloch, J.; Proffen, T.; Billinge, S. PDFfit2 and PDFgui: Computer programs for studying nanostructure in crystals. *J. Phys.: Condens. Matter* **2007**, *19* (33), 335219.
(24) Newville, M. IFEFFIT: Interactive XAFS analysis and FEFF fitting. *J. Synchrotron Radiat.* **2001**, *8*, 322−324.
(25) Lee, Y.; Stephens, P.; Tang, Y.; Li, W.; Phillips, B.; Parise, J.; Reeder, R. Arsenate substitution in hydroxylapatite: Structural characterization of the Ca-5(P*x*As$_1$-*x*O$_4$)(3)OH solid solution. *Am. Mineral.* **2009**, *94* (5−6), 666−675.
(26) Kitahama, K.; Kiriyama, R.; Baba, Y. Refinement of crystal-structure of scorodite. *Acta Crystallogr., Sect. B: Struct. Sci.* **1975**, 322−324.
(27) Spiccia, L.; Marty, W.; Giovanoli, R. Hydrolytic trimer of chromium(III)—Synthesis through chromite cleavage and use in the preparation of the active trimer hydroxide. *Inorg. Chem.* **1988**, *27* (15), 2660−2666.
(28) Spiccia, L.; Marty, W. The fate of active chromium hydroxide, Cr(OH)3.3H$_2$O, in aqueous suspension—Study of the chemical changes involved in aging. *Inorg. Chem.* **1986**, *25* (3), 266−271.
(29) Gao, Y.; Mucci, A. Individual and competitive adsorption of phosphate and arsenate on goethite in artificial seawater. *Chem. Geol.* **2003**, *199* (1−2), 91−109.
(30) Rietra, R.; Hiemstra, T.; Van Riemsdijk, W. Interaction between calcium and phosphate adsorption on goethite. *Environ. Sci. Technol.* **2001**, *35* (16), 3369−3374.
(31) Stachowicz, M.; Hiemstra, T.; van Riemsdijk, W. Multi-competitive interaction of As(III) and As(V) oxyanions with $Ca^{2+}$, $Mg^{2+}$, $PO_4^{3-}$, and $CO_3^{2-}$ ions on goethite. *J. Colloid Interface Sci.* **2008**, *320* (2), 400−414.
(32) Guan, X.; Ma, J.; Dong, H.; Jiang, L. Removal of arsenic from water: Effect of calcium ions on As(III) removal in the KMnO(4)-Fe(II) process. *Water Res.* **2009**, *43* (20), 5119−5128.
(33) Casey, W.; Rustad, J.; Spiccia, L. Minerals as molecules-use of aqueous oxide and hydroxide clusters to understand geochemical reactions. *Chem.—Eur. J.* **2009**, *15* (18), 4496−4515.
(34) Casey, W.; Swaddle, T. Why small? The use of small inorganic clusters to understand mineral surface and dissolution reactions in geochemistry. *Rev. Geophys.* **2003**, *41* (2), 4-1−4-20.